Monthly Notices of the ROYAL ASTRONOMICAL SOCIETY

MNRAS **480,** L116–L120 (2018)
Advance Access publication 2018 July 27

doi:10.1093/mnrasl/sly136

The flux distribution of individual blazars as a key to understand the dynamics of particle acceleration

Atreyee Sinha,[1]† Rukaiya Khatoon,[2]★ Ranjeev Misra,[1] Sunder Sahayanathan,[3] Soma Mandal,[4] Rupjyoti Gogoi[2] and Nilay Bhatt[3]

[1]*Inter-University Center for Astronomy and Astrophysics, Post Bag 4, Ganeshkhind, Pune-411007, India*
[2]*Tezpur University,Napaam-784028, Assam, India*
[3]*Astrophysical Sciences Division, Bhabha Atomic Research Centre, Mumbai - 400085, India*
[4]*Government Girls' General Degree College, Kolkata-700023, West Bengal, India*

Accepted 2018 July 24. Received 2018 July 24; in original form 2018 April 12

The observed lognormal flux distributions in the high-energy emission from blazars have been interpreted as being due to variability stemming from non-linear multiplicative processes generated dynamically from the accretion disc. On the other hand, rapid minute scale variations in the flux point to a compact emitting region inside the jet, probably disconnected from the disc. In this work, we show that linear Gaussian variations of the intrinsic particle acceleration or escape time-scales can produce distinct non-Gaussian flux distributions, including lognormal ones. Moreover, the spectral index distributions can provide confirming evidence for the origin of the variability. Thus, modelling of the flux and index distributions can lead to quantitative identification of the micro-physical origin of the variability in these sources. As an example, we model the X-ray flux and index distribution of Mkn 421 obtained from ∼9 yr of MAXI observations and show that the variability in the X-ray emission is driven by Gaussian fluctuations of the particle acceleration process rather than that of the escape rate.

Key words: acceleration of particles – galaxies: active – BL Lacertae objects: general – BL Lacertae objects: individual: Mkn 421.

1 INTRODUCTION

Blazars are a special class of radio-loud active galactic nuclei (AGNs) and their observed broad-band spectra are dominated by non-thermal emission arising from radiative cooling of relativistic electron distributions in powerful Doppler-boosted jets (Urry & Padovani 1995). Additionally, blazar luminosity is observed to vary over time-scales of years down to minutes and at all wavelengths across the electromagnetic spectrum. Despite many decades of observations, the cause of the underlying variability is poorly understood. The dominance of the non-thermal emission further hinders our understanding of the accretion disc-jet connection in these sources.

Irrespective of the origin, emission from blazars has been found to be stochastic in nature, similar to that seen in other AGNs and Galactic X-ray binaries (McHardy et al. 2006; Chatterjee et al. 2012; Nakagawa & Mori 2013; Sobolewska et al. 2014). Since the past decade, much work has been done to understand the flux distribution of the lightcurves. For a linear stochastic process, a Gaussian distribution of the flux is to be expected, with the width of the distribution determining the flux variation. However, for the case of the eponymous blazar BL Lac, a lognormal flux distribution was clearly evident in the long-term X-ray light curves, with the average amplitude of variability being proportional to the flux level (Giebels & Degrange 2009). Henceforth, this behaviour has been witnessed even in other blazars, and at different timescales and wavelengths (H.E.S.S. Collaboration 2010; Chevalier et al. 2015; Kushwaha et al. 2016; Sinha et al. 2016, 2017; Shah et al. 2018). Such properties were initially observed in the X-ray emission of the galactic black hole binary Cygnus X-1 (Uttley & McHardy 2001), and are usually interpreted as arising from multiplicative processes which originate in the accretion disc (Lyubarskii 1997; Uttley, McHardy & Vaughan 2005; McHardy 2010). However, minute time-scale variability as seen in many blazars (Gaidos et al. 1996; Aharonian et al. 2007; Albert et al. 2007; Paliya et al. 2015) is difficult to originate from the disc (Narayan & Piran 2012), and strongly favours the variability to originate within the jet.

On the other hand, additive processes can also result in such distributions under specific scenarios. Biteau & Giebels (2012) studied the statistical properties of the mini jets-in-a-jet model of Giannios, Uzdensky & Begelman (2009) and showed that the total flux from randomly oriented mini jets will converge to an α-stable

★ E-mail: rukaiyakhatoon12@gmail.com
† Now at: APC, AstroParticule et Cosmologie, Université Paris Diderot, CNRS/IN2P3, CEA/Irfu, Observatoire de Paris, Sorbonne Paris Cité, 10, rue Alice Domon et Léonie Duquet, 75205 Paris Cedex 13, France.

© 2018 The Author(s)
Published by Oxford University Press on behalf of the Royal Astronomical Society

Downloaded from https://academic.oup.com/mnrasl/article/480/1/L116/5060763 by guest on 25 April 2024

distribution. Further, inclusion of experimental uncertainties can imitate such a distribution as a lognormal one. In this work, we provide an alternate interpretation of the non-Gaussian signatures seen in blazar variability through linear fluctuations of the underlying particle acceleration and/or the diffusive escape rate of the emitting electrons. Such small Gaussian perturbations propagate to produce non-linear flux distributions and linear flux-rms relations at high frequencies. This can explain the lognormal behaviour in both the long term stationary time series and during blazar flares, while reproducing the observed flux-rms relations. Finally, this study is used to interpret a plausible cause of variability in light curves obtained from the MAXI observations for the brightest TeV blazar, Mkn 421.

2 PERTURBATION ON THE INTRINSIC TIME-SCALES

We consider a scenario where the non-thermal electrons responsible for the blazar emission are accelerated at a shock front (AR; the acceleration region). Subsequently, they diffuse downstream (CR; the cooling region), at a rate τ_e^{-1}, where they radiate through synchrotron and inverse Compton (IC) mechanisms (Kirk, Rieger & Mastichiadis 1998; Sahayanathan 2008) The kinetic equation describing evolution of the electrons in the AR can be written as (Kardashev 1962)

$$\frac{\partial n(\gamma,t)}{\partial t}+\frac{\partial}{\partial\gamma}\left[\left(\frac{\gamma}{\tau_a}-A\gamma^2\right)n(\gamma,t)\right]+\frac{n(\gamma,t)}{\tau_e}=Q(\gamma), \quad (1)$$

where, γ/τ_a is the electron acceleration rate and $A\gamma^2$ is the radiative loss rate.[1]Together, they govern the maximum attainable Lorentz factor of the accelerated electrons, $\gamma_{max}=\frac{1}{A\tau_a}$. The steady state solution of equation (1) for a mono-energetic electron injection, $Q(\gamma)=Q_0\delta(\gamma-\gamma_0)$, will be

$$n_0(\gamma)=Q_0\tau_a\gamma^{-1-\frac{\tau_a}{\tau_e}}\left(1-\frac{\gamma}{\gamma_{max}}\right)^{\frac{\tau_a}{\tau_e}-1}\left(\frac{1}{\gamma_0}-\frac{1}{\gamma_{max}}\right)^{-\frac{\tau_a}{\tau_e}}. \quad (2)$$

After injection into the CR, the evolution of these particles is governed by

$$\frac{\partial n_s(\gamma,t)}{\partial t}=\frac{\partial}{\partial\gamma}[B\gamma^2 n_s(\gamma,t)]+\frac{n(\gamma,t)}{\tau_e}-\frac{n_s(\gamma,t)}{t_e}, \quad (3)$$

where first term on the right hand side of equation (3) describes the radiative loss rate in the CR, and the last term is the escape of electrons from CR at a rate t_e^{-1}. The steady state solution of the above equation will be a broken power law, with indices τ_a/τ_e + 1 and τ_a/τ_e + 2, and a break at energy $1/Bt_e$. Since the indices of the particle spectrum do not depend on the intrinsic time-scales of the CR, this will not introduce any additional non-linearity in the temporal behaviour. Moreover, as the radiative loss rate is $\propto\gamma^2$, the resultant photon spectrum will again be a broken power law with indices $\tau_a/2\tau_e$ and $(\tau_a+\tau_e)/2\tau_e$ respectively. The narrow width of the single particle emissivity due to synchrotron and inverse Compton emission mechanisms, with respect to the power-law electron distribution, further ensures that the photon spectrum will retain the temporal behaviour of the underlying particle distribution. In addition, the shape of the flux distribution due to synchrotron and inverse Compton scattering of an external photon field will be similar to that of electron number density since the corresponding emissivities are proportional to the number density. On the other hand, for synchrotron self-Compton process, the emissivity will depend on the square of the electron distribution (Sahayanathan, Sinha & Misra 2018) and hence the variance of the distribution will be twice as that of the electron distribution.

[1]Here, the radiative loss includes both synchrotron and inverse Compton processes happening at Thomson regime. For high electron and target photon energies the Compton scattering process will happen at Klein–Nishina regime and the loss rate will be different. However, here we confine or study within the low-energy domain where Thomson approximation is valid.

2.1 Gaussian perturbation on τ_a

A small perturbation in the acceleration time-scale can introduce variation in the accelerated particle number density. If we quantify this variation in τ_a as

$$\tau_a=\tau_{a0}+\Delta\tau_a, \quad (4)$$

where τ_{a0} corresponds to the mean acceleration timescale, the change in the number density can be expressed as

$$\bar{n}(\gamma)=\bar{n}_0(\gamma)+\Delta\bar{n}(\gamma), \quad (5)$$

where $\bar{n}_0$ is the steady state solution (equation 2) corresponding to $\tau_a=\tau_{a0}$. Substituting equations (4) and (5) in the steady state form of equation (1), the fractional variability in $\bar{n}(\gamma)$ can then be obtained as

$$\frac{\Delta\bar{n}(\gamma)}{\bar{n}(\gamma)}=f(\gamma)\frac{\Delta\tau_a}{\tau_a}+g(\gamma)\frac{\Delta\tau_a}{\tau_e}, \quad (6)$$

where

$$f(\gamma)=\left(\frac{1}{1-\gamma/\gamma_{max}}\right) \quad (7)$$

$$g(\gamma)=\log\frac{\gamma_0(1-\gamma/\gamma_{max})}{\gamma(1-\gamma_0/\gamma_{max})}-\frac{\gamma/\gamma_{max}}{1-\gamma/\gamma_{max}}+\frac{\gamma_0/\gamma_{max}}{1-\gamma_0/\gamma_{max}}. \quad (8)$$

From equation (6), it is evident that the variability in $\bar{n}(\gamma)$ is a linear combination of Gaussian and lognormal terms. The relative amplitudes of these terms are decided by the functions $f(\gamma)$ and $g(\gamma)$. For the case $\gamma_{max}\to\infty$, the lognormal term dominates when $\gamma\gg\gamma_0\exp(\tau_e/\tau_a)$. Also in this case, the standard deviation of a normally distributed τ_a will be approximately $\tau_e/\log(\gamma_0/\gamma)$ times that of $\log\bar{n}(\gamma)$. Since the variability in photon index will be equal to $\Delta\tau_a/2\tau_e$, the standard deviation of the logarithm of the photon flux distribution will be $2|\log(\gamma_0/\gamma)|$ times the index distribution (in case of synchrotron and external Compton processes).

To quantify the deviation of $n(\gamma,t)$ from a Gaussian, we simulate its temporal behaviour by solving equation (1) numerically using finite difference scheme. Gaussian perturbations of varying widths (σ_{τ_a}) are then introduced in τ_a and the time series spanning over 5000 points of $n(\gamma)$ is computed for each case at different values of γ. The values of γ_0 and γ_{max} are kept fixed at 10 and 10^5 respectively. The generated time series are then investigated for various statistical properties.

In Fig. 1(a), we plot the skewness of the accelerated electron distribution (κ_n) as a function of σ_{τ_a}/τ_a for different values of γ. Since the fractional variation in the blazar spectral index during different flux states is 15 per cent approximately (see Section 3), we extend σ_{τ_a}/τ_a variation up to 0.25. At low-electron energies ($\gamma\approx30$) the skewness of the distribution is negligible indicating a symmetric distribution. However, the distributions drift towards highly tailed ones for increasing electron energies, thus implying a deviation from Gaussianity. To investigate whether the skewed high-energy electron distribution reflects a lognormal behaviour, we plot in Fig. 1(c), the skewness of the logarithm of the number density

Downloaded from https://academic.oup.com/mnrasl/article/480/1/L116/5060763 by guest on 25 April 2024

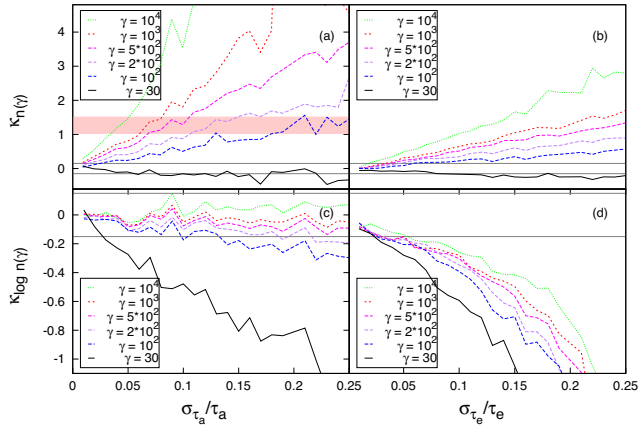

Figure 1. Skewness (κ) of the simulated particle distribution as a function of σ_{τ_a}/τ_a and σ_{τ_e}/τ_e is shown in (a) and (b), whereas the skewness of the logarithm of the distribution as a function of σ_{τ_a}/τ_a and σ_{τ_e}/τ_e is shown in (c) and (d). The solid line corresponds to electron with Lorentz factor $\gamma = 30$ (black), dashed line to $\gamma = 10^2$ (blue), dashed line to $\gamma = 2 * 10^2$ (purple), dashed line to $\gamma = 5 * 10^2$ (magenta), short dashed line to $\gamma = 10^3$ (red) and dotted line $\gamma = 10^4$ (green). The grey lines show the 3-σ ($3\sqrt{15/N}$) error range (Press et al. 1992). The pink band shows the 1-σ error range for the observed value for Mkn421 (Section 3).

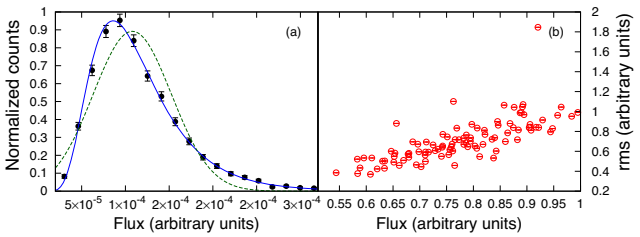

Figure 2. (a) Histogram of the simulated particle number density for $\sigma_{\tau_a}/\tau_a = 0.1$ and $\gamma = 10^3$. The dashed green line represents the best-fitting Gaussian and the solid blue line represents the best-fitting lognormal PDF. (b) The flux-rms scatter plot obtained by dividing the simulated time series into 50 equal time bins. A strong positive correlation is clearly evident ($\rho = 0.83$, $P = 4 \times 10^{-26}$).

($\kappa_{\log n}$) as a function of σ_{τ_a}/τ_a. Here, the skewness is negligible for increasing electron energies suggesting a possible drift towards a lognormal distribution. To confirm this, we further fit the normalized distribution of the number densities with Gaussian and lognormal probability density functions (PDFs). We find that a lognormal PDF significantly fits the distribution better at high-electron energies. In Fig. 2(a), we show the normal and lognormal fit to the electron distribution corresponding to $\gamma = 10^3$ and $\sigma_{\tau_a}/\tau_a = 0.1$. Clearly, the fit statistics is better for a lognormal with a reduced chi-square, $\chi^2_{\rm red} \approx 1.1$ for 17 degrees of freedom (dof), than a Gaussian ($\chi^2_{\rm red} \approx 20.9$ for 17 dof) PDF. The lognormal behaviour of the number density n at large γ lets us express the skewness of the distribution as

$$\kappa_n = \left(2 + e^{\sigma^2_{\log n}}\right) \sqrt{e^{\sigma^2_{\log n}} - 1}, \tag{9}$$

where $\sigma_{\log n}$ is the standard deviation of log n which can be approximated as

$$\sigma_{\log n} \approx \frac{g(\gamma)}{\tau_e} \sigma_{\tau_a}. \tag{10}$$

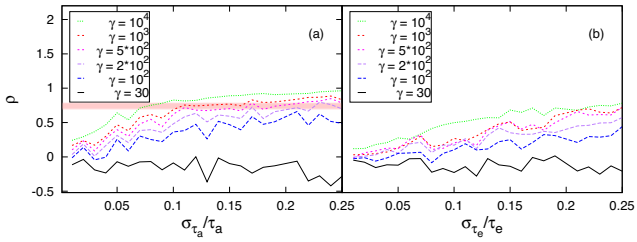

Figure 3. Spearman's rank correlation coefficient ρ of the flux-rms scatter plot as a function of (a) σ_{τ_a}/τ_a and (b) σ_{τ_e}/τ_e. The legends are same as in Fig. 1. The pink band shows the 1-σ ($0.6325/\sqrt{N-1}$) error range for the observed value for Mkn421 (Section 3).

The energy dependence of $\sigma_{\log n}$ will cause the skewness (κ_n) to increase with energy which in turn can be an indicator for the energy of the emitting electrons. It is evident from equations (9) and (10) that for $\sigma_{\tau_a} \to 0$, the distribution of n will closely reflect a Gaussian behaviour.

A necessary feature of a lognormal behaviour is a linear dependence of the average flux on its excess (rms) variation (Vaughan et al. 2003). Consistently, the electron number density at high energies should reflect this behaviour and to examine this, we compute the average number density and its variation, for a given γ and σ_{τ_a}/τ_a, by dividing the corresponding time series into 50 equal time bins. In Fig. 2(b), we show the distribution of the average number density and its variation for $\gamma = 10^3$ and $\sigma_{\tau_a}/\tau_a = 0.1$. A Spearman's rank correlation study shows these quantities are significantly correlated with correlation coefficient $\rho = 0.83$ with null hypothesis probability $P = 4 \times 10^{-26}$. In Fig. 3(a), we plot the correlation coefficient with respect to σ_{τ_a}/τ_a for different values of γ. It can be noted that the correlation improves with the increasing value of γ, thereby supporting a lognormal behaviour.

2.2 Gaussian perturbation on τ_e

In addition to the acceleration rate, the observed photon spectral index will also depend on the confinement time of the electron distribution within AR. In other words, a variation in the escape timescale in AR can introduce non-linearity in the electron distribution. To study this effect, we quantify the variation in escape time-scale (τ_e) in AR as

$$\tau_e = \tau_{e0} + \Delta\tau_e \tag{11}$$

and the corresponding change in the electron number density as

$$\tilde{n}(\gamma) = \tilde{n}_0(\gamma) + \Delta\tilde{n}(\gamma), \tag{12}$$

where $\tilde{n}_0$ is the steady state solution (equation (2)) corresponding to $\tau_e = \tau_{e0}$. Following the procedure similar to the case of τ_a (Section 2.1), substituting equations (11) and (12) in the steady state form of equation (1), the fractional variability in $\tilde{n}(\gamma)$ can then be obtained as

$$\frac{\Delta\tilde{n}}{\tilde{n}} = \tau_a \frac{\Delta\tau_e}{\tau_e^2} f(\gamma), \tag{13}$$

where

$$f(\gamma) = \log \frac{\gamma(1 - \gamma_0/\gamma_{max})}{\gamma_0(1 - \gamma/\gamma_{max})}. \tag{14}$$

It is evident from equation (13), that while the resultant distribution will be neither normal nor lognormal, it will be a skewed one. Additionally, since the particle index $p \sim \frac{\tau_a}{\tau_e}$, the distribution of the spectral indices will also be skewed.

Downloaded from https://academic.oup.com/mnrasl/article/480/1/L116/5060763 by guest on 25 April 2024

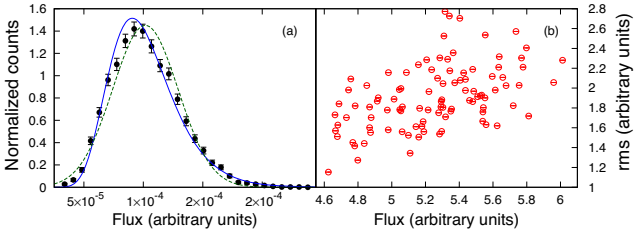

Figure 4. (a) Histogram of the simulated particle number density for $\sigma_{\tau_e}/\tau_e = 0.1$ and $\gamma = 10^3$. The dashed green line represents the best-fitting Gaussian and the solid blue line, the best-fitting lognormal PDF. (b) The flux-rms scatter plot obtained by dividing the simulated time series into 50 equal time bins. A weak positive correlation is seen ($\rho = 0.26$, $P = 0.0071$).

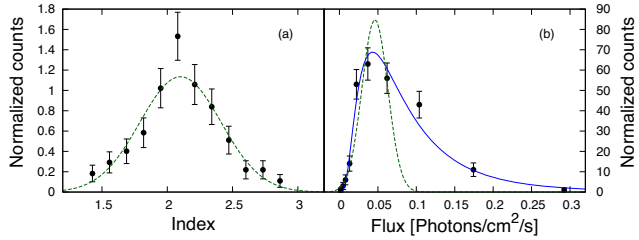

Figure 5. Histograms of the 10 d binned X-ray (a) spectral index at 2–10 keV and (b) 2–20 keV flux of Mkn 421 spanning over 9 yr. The dashed green line corresponds to the best-fitting Gaussian function, whereas the solid blue line corresponds to the best-fitting lognormal one.

To further quantify the effect on the electron number density due to a Gaussian fluctuation in τ_e, we simulate the temporal behaviour of $n(\gamma, t)$ by solving equation (1) numerically (Section 2.1). In Fig. 1(b), we show the skewness of the particle distribution (κ_n) as a function of σ_{τ_e}/τ_e for different values of γ. The distributions are highly tailed for increasing values of γ supporting a non-Gaussian behaviour. A similar behaviour is also observed in case of the skewness of the logarithm of the number density ($\kappa_{\log n}$) which is shown in Fig. 1(d). These studies suggest that the resultant electron number density distribution is significantly skewed; however, it is neither normal nor lognormal.

We also perform the Anderson Darling test on the distribution of the electron number density for various γ. Consistent with our earlier study, both Gaussian and lognormal fits are strongly rejected. In Fig. 4(a), we show the normalized histogram of the electron number density for $\gamma = 10^3$ and $\sigma_{\tau_e}/\tau_e = 0.1$ fitted with Gaussian and lognormal PDFs. Our fit result suggests both of these PDFs cannot represent the given distribution with $\chi^2_{\rm red} \approx 6.7$ (dof=28) for the Gaussian PDF and $\chi^2_{\rm red} \approx 3.7$ (dof = 28) for lognormal one. To study the flux-rms relation, we divide the temporal evolution of the number density into 50 equal time bins (Section 2.1), the average number density and its rms variation corresponding to each bin is determined. In Fig. 4(b), we show their distribution for the case of $\gamma = 10^3$ and $\sigma_{\tau_e}/\tau_e = 0.1$. A Spearman's rank correlation study suggests mild positive correlation between these quantities with $\rho = 0.26$ and $P = 0.0071$. The variation of the flux-rms correlation coefficient with respect to σ_{τ_e}/τ_e is shown in Fig. 3(b) for different values of γ. The correlation improves with increasing value of γ; however, it is less significant than the case of the Gaussian perturbation on τ_a.

3 DISCUSSION

The flux-rms relation of individual blazars or the skewness shown by the distribution of the flux are interpreted by several authors as arising from multiplicative processes, favouring a variability stemming from the disc. Alternatively, Biteau & Giebels (2012) demonstrated that such behaviour can also arise from a collection of randomly oriented mini jets within the jet. They showed that the flux from a randomly oriented mini jet will follow a Pareto distribution which preserves the flux-rms relation. Further, the total flux due to several randomly oriented mini jets will be a sum of Pareto distributions that converge to an α-stable distribution. The resultant flux distribution still holds the flux-rms relation; however, will neither be normal nor lognormal one. Nevertheless, inclusion of experimental uncertainties may imitate the distribution as a lognormal one.

In this work, we show that small temporal fluctuations in the intrinsic time-scales in the AR is capable of producing particle distributions with non-Gaussian signatures and significant flux-rms correlations. The novelty of this work is that it connects the long term temporal behaviour of the blazars with the relatively shorter time-scales of the acceleration process, and provide clues on electron energies responsible for the emission. To highlight this, we study the X-ray observations of the blazar Mkn 421 by *MAXI* satellite, spanning over 9 yr ranging from 2009 to 2018 (Matsuoka et al. 2009). While the integrated counts obtained from a 10 d binned light curve showed a lognormal behaviour with $\chi^2_{\rm red} \approx 1.43$ for 7 dof and $\sigma = 0.33 \pm 0.02$ over a Gaussian one with $\chi^2_{\rm red} \approx 9.84$ for 7 dof (Fig. 5b), the spectral indices estimated from the hardness ratio between 4–10 keV and 2–4 keV fluxes were normally distributed with $\chi^2_{\rm red} \approx 0.81$ for 10 dof, mean $m_p = 2.1 \pm 0.022$ and standard deviation $\sigma_p = 0.31 \pm 0.096$ (Fig. 5a). This suggests that the plausible physical process responsible for the observed flux variation is associated with the fluctuations in the particle acceleration rate. The fractional variation in acceleration time-scale can then be identified from σ_p and m_p of the index distribution as $\sigma_{\tau_a}/\tau_a \approx 0.148 \pm 0.046$. A comparison of Fig. 1(a) with this value and the observed skewness of $\kappa = 1.27 \pm 0.24$ suggests the emission to originate from electrons with γ range $\sim 10^2$–10^3. From Fig. 3(a), we see that this value of γ is consistent with the observed correlation co-efficient $\rho = 0.74 \pm 0.04$. However, this estimate of γ is significantly lower than the electron energies obtained through the broad-band spectral modelling of the source using synchrotron and inverse Compton emission mechanisms (Donnarumma et al. 2009; Abdo et al. 2011; Sinha et al. 2016; Zhu et al. 2016). This discrepancy can be associated with the low value of the injection Lorentz factor γ_0 which is fixed at 10 for this study. From equations (8), (9), and (10), it is evident that the skewness is a function of γ_0/γ rather than γ alone. For a given κ, higher values of γ_0 can result in large γ values that may be consistent with the ones obtained through spectral modelling.

While the lognormal distribution obtained from the light curve of blazars are generally integrated over a certain energy band, here we have quantified the distributions at some fixed electron energy. However, to be consistent with the observations, we verified our results for integrated number densities between different electron energies. We found that our results remain qualitatively similar to that obtained for the case of mono-energetic electron, being strongly dominated by the number counts at the lower energies.

4 CONCLUSION

Through this work, we show that non-Gaussian flux distributions observed in blazars can be associated with the perturbations in the intrinsic time-scales of the main particle acceleration region.

Downloaded from https://academic.oup.com/mnrasl/article/480/1/L116/5060763 by guest on 25 April 2024

A lognormal flux distribution with the spectral indices showing a Gaussian behaviour can be attributed to the fluctuations in the acceleration rate, whereas fluctuations in the electron escape rate can cause flux/index distributions which significantly differ from Gaussian and lognormal ones. Given well sampled multiwavelength lightcurves, this study can be effectively utilized to identify the underlying physical processes, specifically in estimating the fractional fluctuations in the intrinsic time-scales and also the typical electron energies responsible for emission in the different frequency bands. In addition, by a comparison of the flux distributions at different energies (e.g X-ray and gamma-ray), it is possible to identify whether the emission is associated with similar electron energies and thus, constrain spectral models.

ACKNOWLEDGEMENTS

We are thankful to the anonymous referee for valuable comments and suggestions. SM is thankful to ISRO (ISRO/RES/2/404/15-16) and RK is thankful to CSIR, New Delhi (03(1412)/17/EMR-II) for financial support. RG would like to thank IUCAA, Pune for associateship.

REFERENCES

Abdo A. A. et al., 2011, ApJ, 736, 131
Aharonian F. et al., 2007, ApJ, 664, L71
Albert J. et al., 2007, ApJ, 669, 862
Biteau J., Giebels B., 2012, A&A, 548, A123
Chatterjee R. et al., 2012, ApJ, 749, 191
Chevalier J., Kastendieck M. A., Rieger F. M., Maurin G., Lenain J. P., Lamanna G., 2015, in 34th International Cosmic Ray Conference (ICRC2015). p. 829
Donnarumma I. et al., 2009, ApJ, 691, L13
Gaidos J. A. et al., 1996, Nature, 383, 319
Giannios D., Uzdensky D. A., Begelman M. C., 2009, MNRAS, 395, L29
Giebels B., Degrange B., 2009, A&A, 503, 797
H.E.S.S. Collaboration, 2010, A&A, 520, A83
Kardashev N. S., 1962, Sov. Astron., 6, 317
Kirk J. G., Rieger F. M., Mastichiadis A., 1998, A&A, 333, 452
Kushwaha P., Chandra S., Misra R., Sahayanathan S., Singh K. P., Baliyan K. S., 2016, ApJ, 822, L13
Lyubarskii Y. E., 1997, MNRAS, 292, 679
Matsuoka M. et al., 2009, PASJ, 61, 999
McHardy I., 2010, in Belloni T., ed., Lecture Notes in Physics , Springer Verlag, Berlin p. 203
McHardy I. M., Koerding E., Knigge C., Uttley P., Fender R. P., 2006, Nature, 444, 730
Nakagawa K., Mori M., 2013, ApJ, 773, 177
Narayan R., Piran T., 2012, MNRAS, 420, 604
Paliya V. S., Böttcher M., Diltz C., Stalin C. S., Sahayanathan S., Ravikumar C. D., 2015, ApJ, 811, 143
Press W. H., Teukolsky S. A., Vetterling W. T., Flannery B. P., 1992, Numerical recipes in FORTRAN. The art of scientific computing, Cambridge Univ. Press, Cambridge
Sahayanathan S., 2008, MNRAS, 388, L49
Sahayanathan S., Sinha A., Misra R., 2018, RAA, 18, 035
Shah Z., Mankuzhiyil N., Sinha A., Misra R., Sahayanathan S., Iqbal N., 2018, preprint (arXiv:1805.04675)
Sinha A. et al., 2016, A&A, 591, A83
Sinha A., Sahayanathan S., Acharya B. S., Anupama G. C., Chitnis V. R., Singh B. B., 2017, ApJ, 836, 83
Sobolewska M. A., Siemiginowska A., Kelly B. C., Nalewajko K., 2014, ApJ, 786, 143
Urry C. M., Padovani P., 1995, PASP, 107, 803
Uttley P., McHardy I. M., 2001, MNRAS, 323, L26
Uttley P., McHardy I. M., Vaughan S., 2005, MNRAS, 359, 345
Vaughan S., Edelson R., Warwick R. S., Uttley P., 2003, MNRAS, 345, 1271
Zhu Q., Yan D., Zhang P., Yin Q.-Q., Zhang L., Zhang S.-N., 2016, MNRAS, 463, 4481

This paper has been typeset from a TEX/LATEX file prepared by the author.

Downloaded from https://academic.oup.com/mnrasl/article/480/1/L116/5060763 by guest on 25 April 2024